Wind and Structures, *Vol. 24, No. 4 (2017) 385-403*
DOI: https://doi.org/10.12989/was.2017.24.4.385

Hybrid bolt-loosening detection in wind turbine tower structures by vibration and impedance responses

Tuan-Cuong Nguyen[1a], Thanh-Canh Huynh[1b], Jin-Hak Yi[2c] and Jeong-Tae Kim[*1]

[1]*Department of Ocean Engineering, Pukyong National University, Nam-gu, Busan, Korea*
[2]*Coastal and Environmental Engineering Division, Korea Institute of Ocean Science and Technology, Ansan, Gyeonggi-do, Korea*

(Received November 30, 2016, Revised March 8, 2017, Accepted March 21, 2017)

Abstract. In recent years, the wind energy has played an increasingly important role in national energy sector of many countries. To harvest more electric power, the wind turbine (WT) tower structure becomes physically larger, which may cause more risks during long-term operation. Associated with the great development of WT projects, the number of accidents related to large-scaled WT has also been increased. Therefore, a structural health monitoring (SHM) system for WT structures is needed to ensure their safety and serviceability during operational time. The objective of this study is to develop a hybrid damage detection method for WT tower structures by measuring vibration and impedance responses. To achieve the objective, the following approaches are implemented. Firstly, a hybrid damage detection scheme which combines vibration-based and impedance-based methods is proposed as a sequential process in three stages. Secondly, a series of vibration and impedance tests are conducted on a lab-scaled model of the WT structure in which a set of bolt-loosening cases is simulated for the segmental joints. Finally, the feasibility of the proposed hybrid damage detection method is experimentally evaluated via its performance during the damage detection process in the tested model.

Keywords: structural health monitoring; wind turbine tower; hybrid damage detection system; vibration responses; impedance responses

1. Introduction

Over the past few decades, many severe accidents WT structures have been recognized in the world (Ishihara *et al*. 2005, Chou and Tu 2010, Lee and Bang 2012, Chiang *et al*. 2016). Under the long-term operational service, the damage could occur at any component or part of the WT system such as concrete foundation, tower structure, rotor and generator, nacelles and even the electrical subsystems. From 2006 to 2015, statistical data recorded by Caithness Windfarm Information Forum (2016) indicated that the structural failure and the blade failure averagely accounted for more than 25% of

*Corresponding author, Professor, E-mail: idis@pknu.ac.kr
[a]Graduate Student, E-mail: ce.cuongnt@gmail.com
[b]Post-Doctoral Fellow, E-mail: ce.huynh@gmail.com
[c]Principal Research Scientist, E-mail: yijh@kiost.ac.kr

http://www.techno-press.com/journals/was&subpage=7 ISSN: 1226-6116 (Print), 1598-6225 (Online)

total failure types occurred in the WT. It is a fact that the undetected damage such as small cracks can propagate into the sudden failure or the collapse of the WT. Therefore, a SHM system for WT structures is needed to ensure the structural reliability, to minimize maintenance cost, and to prevent catastrophic accidents in the future.

In general, SHM can be classified into two categories: global SHM and local SHM. Thereby, the global SHM is usually utilized to assess the structural integrity of a whole structure. Meanwhile, the local SHM is found to be suitable for damage monitoring at some local subsystem or critical connection members. By using the global SHM concept, many practices have been applied to various structures ranging from bridges to high-rise buildings. However, not many studies related to SHM for the WT system were found. Only a few SHM attempts have been carried out to monitor the in-service WT tower structures by using global approaches. Bang *et al.* (2012) used arrayed fiber Bragg grating sensors to measure strain and bending deflection of a wind turbine tower. Mostböck and Petryna (2014) applied the GPS (global positioning system) technique to monitor the dynamic displacement at various locations on the WT tower. Nguyen *et al.* (2015) investigated the feasibility of vibration-based damage detection in WT structures via finite element modelling. Ebert (2016) developed a laser Doppler vibrometer to measure the vibration of rotating blades of wind turbines up to a distance of several hundred meters. Despite those efforts, intensive researches on the global damage monitoring of WT tower structures are still needed, especially using experimental vibration responses.

Unlike the global SHM, the local SHM for WT's structural members has been received the early attention during the last few decades. Accordingly, many nondestructive evaluation methods, such as acoustic emission method, thermal imaging method, ultrasonic method, electrical resistance-based damage detection method, vision-based method, X-ray method, electro-mechanical impedance-based method have recently been investigated for the local SHM on WT structures (Joosse *et al.* 2002, Lading *et al.* 2002, Dutton 2004, Matsuzaki and Todoroki 2006, Pitchford *et al.* 2007, Park *et al.* 2015). However, these local SHM techniques were mostly developed to focus on detecting structural damage in the blades of wind turbines, and their applications to the critical joints of WT towers are still limited. Among those, the impedance-based method has shown its promising approach to capture the minor changes in structure induced by damage (Park *et al.* 1999, Tseng and Wang 2005, Kim *et al.* 2006, Huynh and Kim 2014, 2016). The method can detect a wide range of structural damage and it is capable for real-time online monitoring. Importantly, the impedance method itself, using high-frequency responses, is less sensitive to operational vibrations. Thus, the impedance-based method would be very potential to be implemented for the damage detection in WT structures in which the rotating blades and the rotors could cause significant noises in the measured dynamic signals.

On the other hand, the combination of the global SHM and the local SHM, so-called the hybrid SHM, was also gained much attention from researchers and scientific community. By adopting the hybrid SHM concept, many research groups have attempted to develop the more efficient methods for monitoring the structural integrity by combining two or more damage detection techniques, such as hybrid piezoelectric/fiber optic (Qing *et al.* 2005, Barazanchy *et al.* 2014), mutual strain's properties measured from optical fiber sensors (Studer and Peters 2004), combined acceleration/strain responses in wavelet-based approach (Law *et al.* 2005), integrated vibration-based/infrared imaging technique (Han *et al.* 2007), hybrid acceleration-impedance-based techniques (Kim *et al.* 2010, Kim *et al.* 2011). These previous studies demonstrated that the hybrid method can provide a better damage monitoring opportunity for SHM as compared to the single approach.

Based on the hybrid health monitoring system by Kim *et al.* (2010), this study presents a modified hybrid approach for bolt-loosening detection in WT tower structures by measuring vibration and impedance responses. The proposed hybrid damage detection scheme utilizes vibration-based and impedance-based methods as a sequential procedure. The feasibility of the proposed approach is examined on a lab-scaled model of the WT structure under various bolt-loosening scenarios of the segmental joints.

2. Hybrid damage monitoring system for WT structure

2.1 Design of hybrid damage monitoring scheme

A hybrid scheme is developed for damage detection in wind turbine (WT) structures by using vibration and impedance responses. As shown in Fig. 1, the damage monitoring process is sequentially implemented in the following three stages: global vibration-based damage occurrence alarming (Stage 1); impedance-based damage classification (Stage 2); and damage location estimation for entire structures (Stage 3).

In Stage 1, the presence of damage is alarmed globally by using the variation of frequency responses. A damage alarming method, which is frequency-response-ratio assurance criterion (FRRAC) described in Section 2.2, is utilized to determine the occurrence of damage in the structure. In Stage 2, once the damage occurrence in target structure is alerted, the impedance-based technique is activated to classify the alerted damage. By using the changes in electro-mechanical (EM) impedance signals, as described in Section 2.3, the alarmed damage is classified into: damage occurred at critical members (i.e., bolted-connection joints) or other locations in

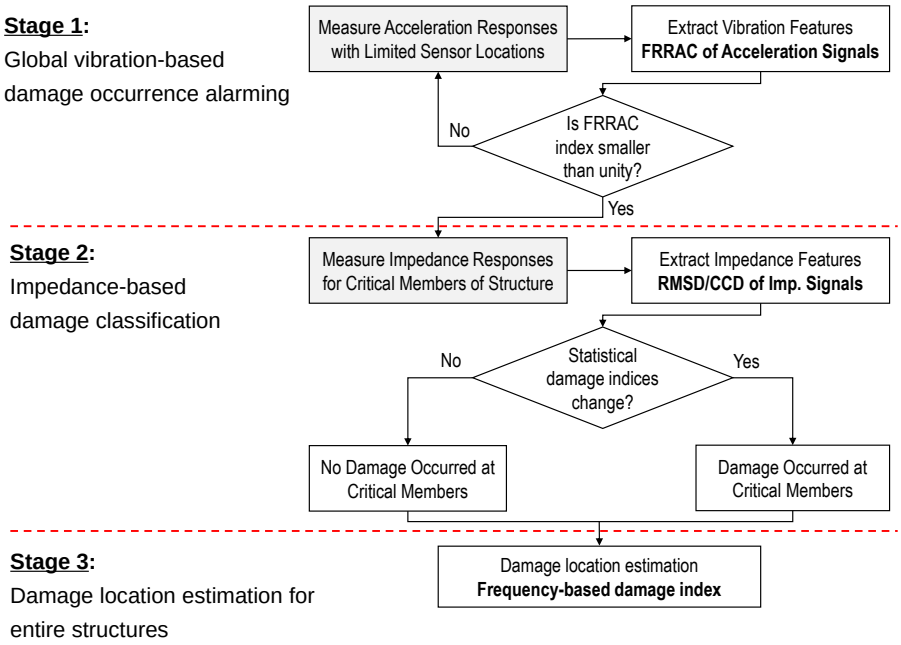

Fig. 1 Hybrid damage monitoring scheme for WT tower structures

the WT tower structure. The statistical damage indices, such as root mean square deviation (RMSD) and correlation coefficient deviation (CCD), are employed to quantify the variation of impedance signatures. In Stage 3, the damage location is predicted for the entire WT tower structure by using frequency-based damage index method, as described in Section 2.4. This step also confirms the damage detection results predicted in Stage 2, and also predicts the other potential damage locations.

It is noted that the damage monitoring process could be completed after finishing Stage 2. However, in reality, the severe damage in the WT tower's segment can be caused by the small cracks during long-term operation. Therefore, the WT tower structure needed to be intensively investigated in Stage 3 to ensure that the potential risks can be covered by the hybrid damage detection system. This is the main difference between the proposed hybrid scheme and the previous one by Kim *et al.* (2010).

2.2 Vibration-based damage occurrence alarming method

Global vibration-based damage occurrence alarming is mainly performed by using FRRAC. The FRRAC was first proposed by Kim *et al.* (2010). It should be noted that the frequency response function (FRF) is defined as a relationship between the input force and the output structural response which was transformed into frequency domain (Bendat and Piersol 1993). Moreover, the output structural response is a function of structural parameters such as mass, damping and stiffness. Therefore, it is feasible to monitor damage induced by changes in physical properties of the structure. The frequency-response-ratio (FRR) is defined for two consecutive locations *i* and *i+1* on the target structure, as follows

$$FRR_{i,i+1}(\omega_z) = \frac{H_i(\omega_z)}{H_{i+1}(\omega_z)} = \frac{ASD_{i,i}(\omega_z)}{CSD_{i,i+1}(\omega_z)} = \frac{E[V_i^*(\omega_z)V_i(\omega_z)]}{E[V_i^*(\omega_z)V_{i+1}(\omega_z)]} \tag{1}$$

where $ASD_{i,i}(\omega_z)$ and $CSD_{i,i+1}(\omega_z)$ are the auto-spectral and cross-spectral density functions, respectively. The influence of external excitations on the FRFs can be ignored by using the FRR.

By comparing the FRR between undamaged and corresponding damage states, the FRRAC index is formulated, as follows

$$FRRAC(u,d) = \frac{[FRR_u^T FRR_d]^2}{[FRR_u^T FRR_u][FRR_d^T FRR_d]} \tag{2}$$

where the subscripts *u* and *d* signify the undamaged state and corresponding damage one, respectively. As expressed in Eq. (2), the FRRAC index is basically utilized to estimate the linear relationship between two FRR vectors. In other words, it also indicates for the degree of consistency between a pair of vectors. Usually, the FRR of undamaged state is chosen as a reference for this estimation. Therefore, the FRRAC index remains close to unity if there is no damage. Otherwise, the FRRAC index decreases from unity if damage occurs.

2.3 Impedance-based damage classification method

Damage classification is performed by using impedance-based monitoring techniques. The impedance-based damage monitoring method was first proposed by Liang *et al.* (1994). The

principle idea of this technique is that the changes in the structure's mechanical impedance represent for the structural failure of monitored zone. In this method, a piezo-electric patch (i.e., PZT patch) is utilized as an actuator to excite the host structure and a sensor to measure the structural responses. According to 1-D model of the interaction between surface-bonded PZT patch and host structure developed by Liang *et al.* (1996), the EM impedance can be expressed, as follows

$$Z(\omega)=\frac{V(\omega)}{I(\omega)}=\left\{i\omega a\left[\hat{\varepsilon}_{33}^{T}-\frac{1}{Z_a(\omega)/Z_s(\omega)+1}d_{3x}^{2}\hat{Y}_{xx}^{E}\right]\right\}^{-1} \tag{3}$$

where $V(\omega)$ is the input harmonic voltage to excite the PZT patch; $I(\omega)$ is the electric current; $Z_a(\omega)$ and $Z_s(\omega)$ are the mechanical impedances of the PZT patch and the host structure, respectively; $\hat{Y}_{xx}^{E}=(1+i\eta)Y_{xx}^{E}$ is the complex Young's modulus of the PZT patch at zero electric field; $\hat{\varepsilon}_{xx}^{T}=(1-i\delta)\varepsilon_{xx}^{T}$ is the complex dielectric constant at zero stress; d_{3x} is the piezoelectric coupling constant in x-direction at zero stress; and a is the geometry constant of the PZT patch. The parameters η and δ are structural damping loss factor and dielectric loss factor of piezoelectric material, respectively. Note that $Z_s(\omega)$ is a function of structural properties, such as mass, damping and stiffness.

As expressed in Eq. (3), the EM impedance depends on the mechanical impedance of not only the PZT patch but also the monitored region. Since the mechanical property of PZT patch is assumed to be unchanged during inspection time, Eq. (3) clearly shows that the change in mechanical impedance of the host structure caused by the changes in structural parameters is directly related to the variation of EM impedance. This point is the key issue to apply the impedance technique on damage monitoring works.

In general, the statistical damage indices, such as RMSD and CCD, are usually used to quantify the changes of impedance signatures. The RMSD index is calculated as follows (Sun *et al.* 1995)

$$RMSD\left(Z,Z^{*}\right)=\sqrt{\frac{\sum_{i=1}^{n}\left[\mathrm{Re}(Z^{*}(\omega_i))-\mathrm{Re}(Z(\omega_i))\right]^{2}}{\sum_{i=1}^{n}\left[\mathrm{Re}(Z(\omega_i))\right]^{2}}} \tag{4}$$

where $\mathrm{Re}(Z(\omega_i))$ and $\mathrm{Re}(Z^{*}(\omega_i))$ are the real components of the impedance signatures measured before and after the damage of the frequency i^{th}, respectively. Also, n denotes the number of frequency points in the sweep band.

On the other hand, the CCD index is calculated as follows (Zagrai and Giurgiutiu 2001)

$$CCD=1-\frac{1}{\sigma_Z\sigma_{Z^{*}}}E\left\{\left[\mathrm{Re}(Z_i)-\mathrm{Re}(\bar{Z})\right]\left[\mathrm{Re}(Z_i^{*})-\mathrm{Re}(\bar{Z}^{*})\right]\right\} \tag{5}$$

where $E[.]$ is the expectation operation; σ_Z and $\sigma_{Z^{*}}$ denote the standard deviation; $\bar{Z}$ and $\bar{Z}^{*}$ denote the mean value of impedance signatures before and after damage, respectively.

As expressed in Eqs. (4) and (5), the statistical damage indices remain close to 0 if no damage. Otherwise, those values are larger than 0. Generally, the CCD index is sensitive with horizontal shifts and less sensitive with vertical shifts of impedance responses. Meanwhile, the RMSD index

is sensitive to both changes of impedance responses. In this study, both quantified approaches are used to ensure that any changes in impedance responses can be captured. According to the above statistical analysis approaches, the alarmed damage can be classified as: damage at critical members or not. If damage indices increase from 0, damage occurs at critical members. Otherwise, there is no damage at those locations.

2.4 Damage location estimation method

By using changes in natural frequencies, a frequency-based damage detection algorithm for structural system of NE elements (j=1, 2,…, q,…, NE) and a set of NM measurable vibration modes (i=1, 2,…, m, n,…, NM) was proposed by Kim *et al.* (2003). For all available vibrational modes, a damage index for location j^{th} (DI_j) can be defined as follows

$$DI_j = \left[\sum_{i=1}^{NM} e_{ij}^2 \right]^{-1/2} \tag{6}$$

where $0 \le DI_j \le \infty$. If this value approaches the local maximum point, it implies that location j^{th} is damaged. Here, the term e_{ij} represents localization error for the location j^{th} that can be measured by using the modal information i^{th}

$$e_{ij} = Z_i \Big/ \sum_{k=1}^{NM} Z_k - F_{ij} \Big/ \sum_{k=1}^{NM} F_{kj} \tag{7}$$

According to Eq. (7), the index e_{ij}=0 implies that location j^{th} can be damaged. By ignoring changes in mass due to damage, the term Z_i is the fractional change in the eigenvalue i^{th}, which is given as

$$Z_i = \left(\omega_i^{*2} - \omega_i^{\,2} \right) \Big/ \omega_i^{\,2} \tag{8}$$

where the asterisk represents for damage state. On the other hand, the term F_{ij} is the modal sensitivity of the mode i^{th} and the element j^{th}, which is defined by an alternative way as

$$F_{ij} = \int_j EI \left[\Phi_i^{"}(\mathrm{x}) \right]^2 dx \Big/ \int_0^L EI \left[\Phi_i^{"}(x) \right]^2 dx \tag{9}$$

where E is elastic's modulus; I is the inertial moment of cross-section of equivalent beam; and $\Phi_i^{"}(x)$ is the mode-shape curvatures. By treating the damage index (DI) values computed by using Eq. (6) as random variables, they are normalized according to standard rule as

$$Z_j = \left(DI_j - \mu_{DI} \right) / \sigma_{DI} \tag{10}$$

where μ_{DI} and σ_{DI} are the mean and the standard deviation of the sample of damage indices, respectively. Hence, the damage is identified the statistical hypothesis tests. A complete description of this technique can be found in the literature (Kim *et al.* 2003).

3. Experiment on WT tower model

3.1 Experimental Setup

A lab-scaled WT tower model consisting of three 0.5 m-stainless steel segments was selected as the test structure (see Fig. 2). As shown in Fig. 2(a), the tower structure was placed on the steel base plate, which was supported by a concrete foundation, via the bolted-connection at the bottom joint. A 300-watt motor of an electrical fan placed at the top of the tower was chosen as the rotor for this model. With this assembling, the test structure height was approximately 1.85 m. The electric fan was designed to operate with two wind velocities, 6.67 m/s and 9.94 m/s.

In the WT tower model, the tower's segments were made by rectangular hollow cross-sections and they were linked by bolted-connections. The bolted-connection was manufactured by two steel splice plates with four fastened-bolts. Typical bolted-connection joints of Joint D (Top) and Joint A (Bottom) were shown in Figs. 2(b) and 2(c), respectively. The sketch of sensor deployment on the test structure was presented in Fig. 3. The sensor's arrangements in side view and plan view were sketched in Figs. 3(a) and 3(b), respectively. In all joints, the bolts were numbered sequentially in a clockwise direction, as depicted in Fig. 3(b).

For acceleration measurement, five commercial accelerometers (Acc. #1-#5) were placed on Joint A to Joint D along the z-direction, as depicted in Fig. 3. Note that 2 accelerometers (Acc. #1-#2) were used at Joint D for recognizing the twist motion of the tower which might be caused by the mass eccentricity during the forced vibration test. A type of ICP accelerometer was used in the test: PCB 333B52 with a nominal sensitivity of 1 V/g and a specified frequency range of 0.5-3 kHz.

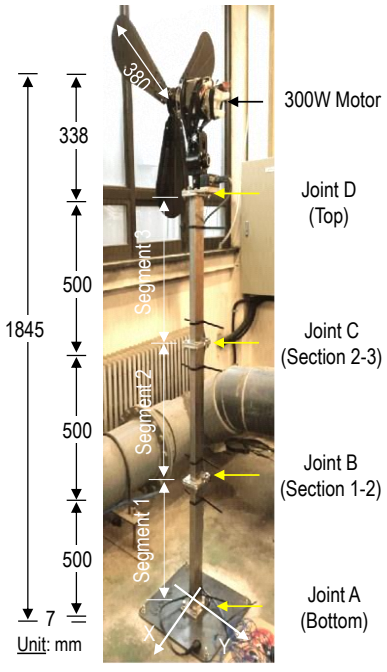

(a) Tower structure

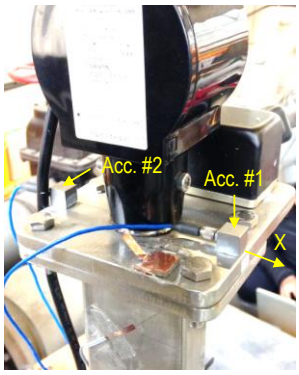

(b) Joint D (Top)

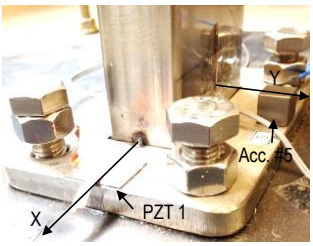

(c) Joint A (Bottom)

Fig. 2 Lab-scaled WT model

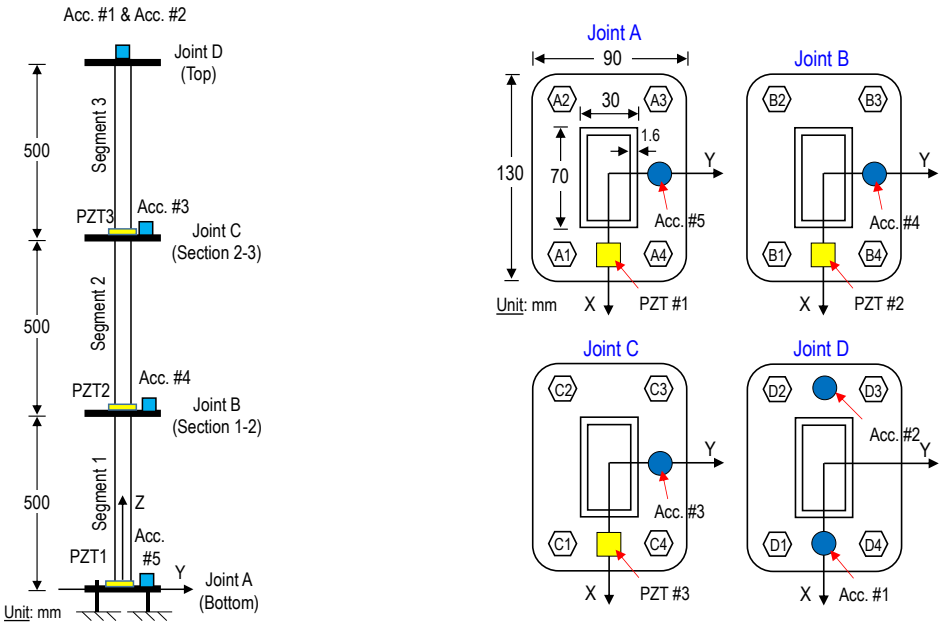

(a) Side view (b) Plan view

Fig. 3 Sensor deployment on the tested model

Table 1 Damage cases performed on lab-scaled WT tower model

Damage location	Damage case	Damage simulation on the tested model
Joint A (Bottom)	Reference (A)	All bolts are fastened as the intact condition
	Bolt A1	Bolt A1 is completely loosened
	Bolts A1_A3	Additional Bolt A3 is completely loosened.
Joint B (Section 1-2)	Reference (B)	All bolts are refastened as the intact condition
	Bolt B1	Bolt B1 is completely loosened
	Bolts B1_B3	Additional Bolt B3 is completely loosened
Joint C (Section 2-3)	Reference (C)	All bolts are refastened as the intact condition
	Bolt C1	Bolt C1 is completely loosened
	Bolts C1_C3	Additional Bolt C3 is completely loosened
Joint D (Top)	Reference (D)	All bolts are refastened as the intact condition
	Bolt D1	Bolt D1 is completely loosened
	Bolts D1_D3	Additional Bolt D3 is completely loosened

The accelerometers were fixed on the top surface of the bolted-connection. The specified locations of acceleration sensors were selected to measure flexural vibration modes as distinct to twist (torsional) modes. Uncontrolled impact-forces were applied in the *y*-direction at the joint B (Section 1-2) (i.e., 0.5 m distanced from the steel base plate). The data acquisition system known as 8-channel HBM's QuantumX-MX840A was employed to obtain the acceleration signals. The sampling frequency was set as 300 Hz. By using the stochastic subspace identification (SSI)

method, the modal parameters such as natural frequencies, mode-shapes, damping ratio were extracted from the *y*-directional acceleration responses (Overschee and De Moor 1996).

For impedance measurement, three PZT patches (PZT #1-#3) were directly bonded on the top surface of the steel connection plate. As depicted in Fig. 3, the PZT sensors were located at three joints: Joint A (Bottom), Joint B (Section 1-2) and Joint C (Section 2-3). So the local sensitive impedance responses were measured only for the three connections. A data acquisition system consisting of an impedance analyzer HIOKI 3532 and a computer with LabVIEW software was used to measure the electrical impedance signals. In trial and error, the frequency range of 100 kHz-300 kHz was found sensitive for damage monitoring jobs at the bolted-connection joint than other ranges. The input voltage set to excite the PZT sensors was 1 V. The output signals from the sensor were acquired to extract frequency-domain impedance signatures. During experimental tests, a system with K-type thermocouple wire and KYOWA (EDX-100A) Temperature Logger was utilized to measure the room's temperature. Accordingly, the temperature was controlled as close as constant at 18°C by air conditioners.

3.2 Experimental modal tests

A series of forced vibration tests were performed on the WT tower model. Two levels of damage were inflicted on each of the four bolted-connection joints. For each joint, the procedure for loosening bolts was implemented by two steps: (1) all four bolts were securely fastened; (2) a bolt (#1) was completely loosened; and (3) another bolt (#3) was subsequently unfastened. After measuring vibration and impedance responses, the loosened bolts were retightened back to the intact condition. This procedure was repeated for all four bolted-connection joints (from Joint A to Joint D). Totally eight single damage cases were simulated in the lab-scaled WT model, as listed in Table 1.

4. Hybrid bolt-loosening monitoring on WT tower model

4.1 Vibration-based damage occurrence alarming (Stage 1)

As the first stage (Stage 1) of the hybrid damage monitoring practice described in Fig. 1, the damage occurrence alarming for the WT tower model was performed as follows. The auto-spectral density function, *ASD*(4,4), and the cross-spectral density function, *CSD*(4,5) were computed from acceleration signals measured by sensors #4 and #5. According to Eq. (1), FRR is the frequency-response-ratio for any two consecutive sensors. In reality, the accelerometers installed near the top of WT towers can be affected by the vibration of blades and rotor which could cause significant noises in measured acceleration signals. Therefore, the two consecutive sensors #4 and 5# which are close to the bottom of the WT tower were selected for the calculation of FRR. By using Eq. (1), the frequency-response-ratio function, *FRR*(4,5), was obtained for the reference (undamaged case) and the corresponding damage cases. Then frequency-response-ratios were computed for all damage cases. Fig. 4 illustrates for damage alarming process at joint A. The damage-induced variation is observed in the auto-spectral density - ASD, the cross-spectral density - CSD, and the frequency-response-ratio - FRR.

By using Eq. (2), the FRRAC values were calculated for all damage locations (i.e., Joints A-D). For each damage location, the FRR function of the reference case was set as the baseline for this

evaluation. As shown in Fig. 5, it is clear that the FRRAC values were decreased from the unity. For all bolt-loosening cases, the FRRAC indices successfully alerted the damage.

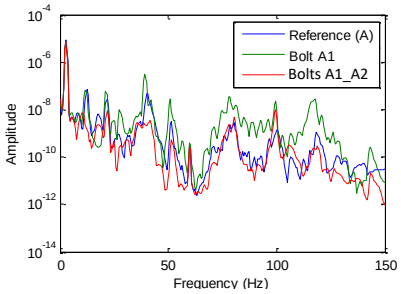

(a) Auto-spectral density - ASD(4,4)

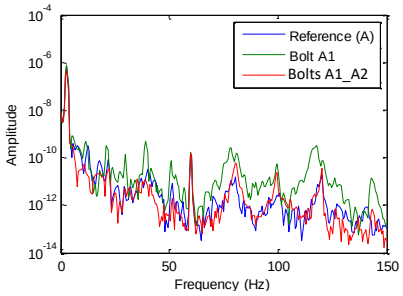

(b) Cross-spectral density - CSD(4,5)

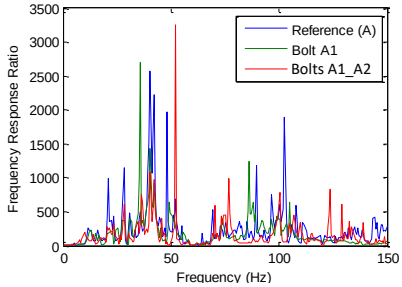

(c) Frequency-response-ratio - FRR(4,5)

Fig. 4 Frequency-response-ratio by sensors #4 and #5 for damage cases at Joint A (Bottom)

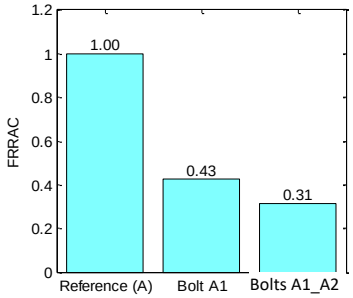

(a) Joint A (bottom)

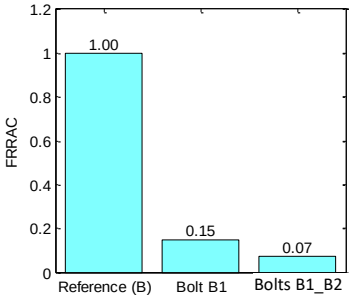

(b) Joint B (Section 1-2)

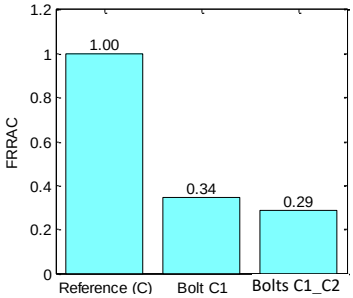

(c) Joint C (Section 2-3)

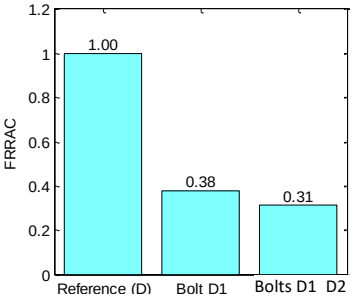

(d) Joint D (Top)

Fig. 5 Damage occurrence alarming by FRRAC index for all damage cases

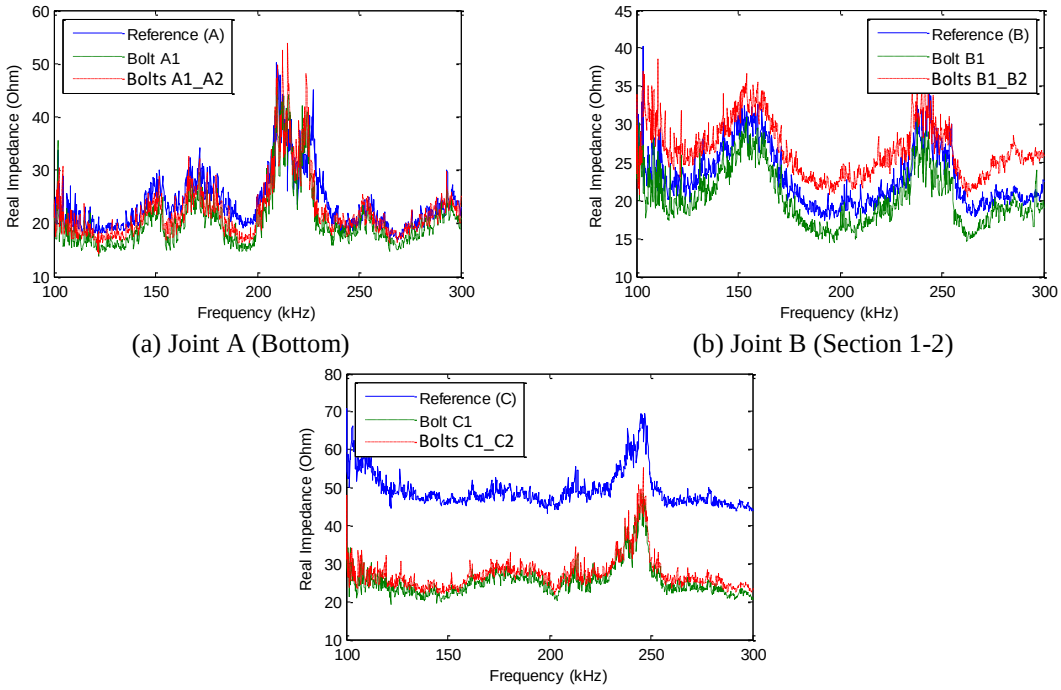

(a) Joint A (Bottom)

(b) Joint B (Section 1-2)

(c) Joint C (Section 2-3)

Fig. 6 Real impedance signatures measured before and after damage

4.2 Impedance-based damage classification (Stage 2)

Once the presence of damage was alerted globally, the damage was classified as one of potential damage locations (e.g., segmental joints where the PZT sensors were installed) by using the impedance-based technique (Stage 2) as designed in Fig. 1. The integrity of the bolted-connection joint can be monitored sensitively since any change in the sensor-vicinity region can be measured by the change in the impedance signature out of the embedded PZT patch. As shown in Fig. 6, the real parts of impedance responses were measured from the PZT sensors installed at the three joints (i.e., Joints A, B and C).

For example, Fig. 6(a) show the impedance signatures of 100-300 kHz range measured at Joint A before and after the two bolt-loosening events, as described in Table 1. It is worth noticing that some resonant peaks are observed in the selected frequency range. As observed in Fig. 6(a), the noticeable changes in real impedance responses due to the bolt-loosening events was the magnitude while the changes in the resonance peaks were not quite clearly observed.

As shown in Fig. 7, the changes in real impedance responses were quantified by the RMSD and CCD indices, respectively. For all damage locations (i.e., Joints A, B and C), both the RMSD and CCD indices were increased significantly from zero as the bolt-loosening events were conducted. Both RMSD and CCD indices were successful in indicating bolt-loosening at the bolted-connection joints. Compared to the RMSD indices, the CCD indices increased proportionally as the development of the damage severity. It is noted that using CCD index can be better than using RMSD index to quantify the changes in impedance responses.

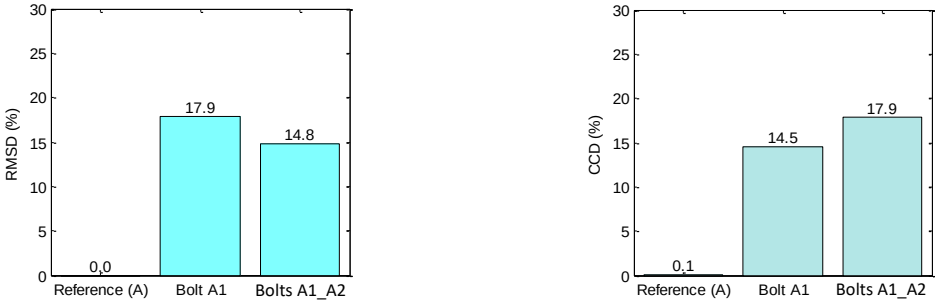

(a) RMSD and CCD indices at Joint A (Bottom)

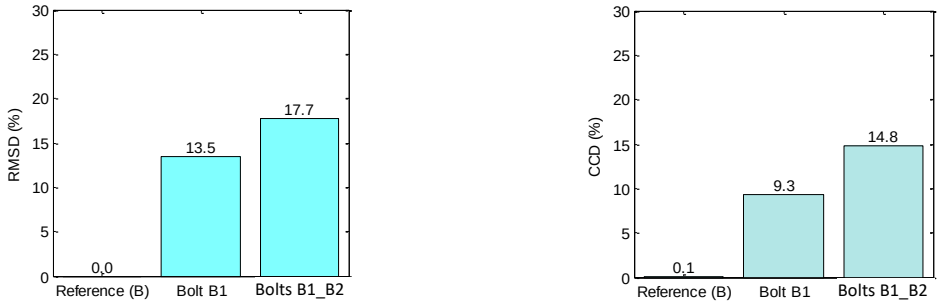

(b) RMSD and CCD indices at Joint B (Section 1-2)

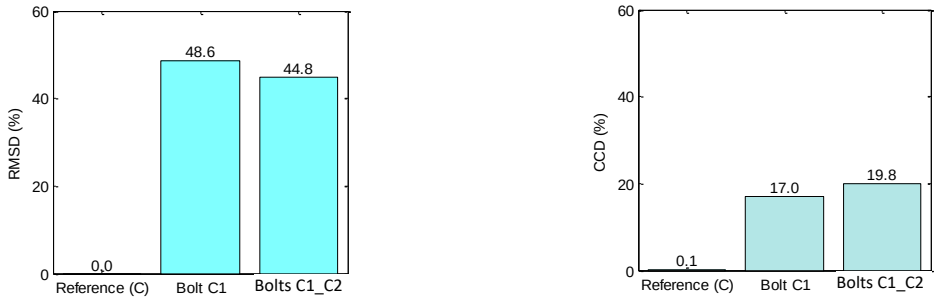

(c) RMSD and CCD indices at Joint C (Section 2-3)

Fig. 7 Damage classifications by impedance-based technique

4.3 Damage location estimation (Stage 3)

As the final stage (Stage 3) of the hybrid monitoring, the frequency-based damage detection algorithm was utilized to estimate damage location for entire the WT tower structure. The damage location estimation was performed by using natural frequencies of the first three bending modes (as listed in Table 2) measured before and after bolt-loosening episodes. Then, the relative changes in eigenvalues, Z_i, were calculated by using Eq. (8) for each damage case.

Next, the modal sensitivities, F_{ij}, were calculated by using Eq. (9). A finite element (FE) model of the tested structure was required to construct the numerical modal sensitivity matrix. As shown in Fig. 8, the FE model and its three bending mode shapes were analyzed by using a commercial software, MIDAS FEA. Geometries of the numerical model were based on the real dimensions of the lab-scaled model. By idealizing the WT structure as a cantilever beam with the added mass at

the free end, the total mass of motor and blades could be lumped into the top plate at a location 0.07 m distanced from the central axis, as described in Fig. 8. The connection between the bottom plate and the steel base plate was assumed as fixed by four rigid links. Material properties of FE model were defined for stainless steel as: elastic's modulus E=198 GPa, mass density ρ=7880 kg/m^3 and Poisson's ratio ν=0.3.

Table 2 Natural frequencies before and after bolt-loosening extracted by SSI method

Damage location	Damage case	Natural frequency (Hz)		
		Mode 1	Mode 2	Mode 3
Joint A (Bottom)	Reference (A)	2.8243	40.1203	100.4870
	Bolt A1	2.8012	39.4765	99.6226
	Bolts A1_A3	2.7847	38.8231	99.4590
Joint B (Section 1-2)	Reference (B)	2.8161	39.8182	100.2238
	Bolt B1	2.7532	39.6811	98.0365
	Bolts B1_B3	2.7293	39.6994	97.3841
Joint C (Section 2-3)	Reference (C)	2.8314	40.0145	100.3649
	Bolt C1	2.8206	39.4516	100.0515
	Bolts C1_C3	2.8156	39.3935	98.7509
Joint D (Top)	Reference (D)	2.8564	40.7390	102.7893
	Bolt D1	2.8506	40.7311	102.3503
	Bolts D1_D3	2.8509	40.6445	101.4162

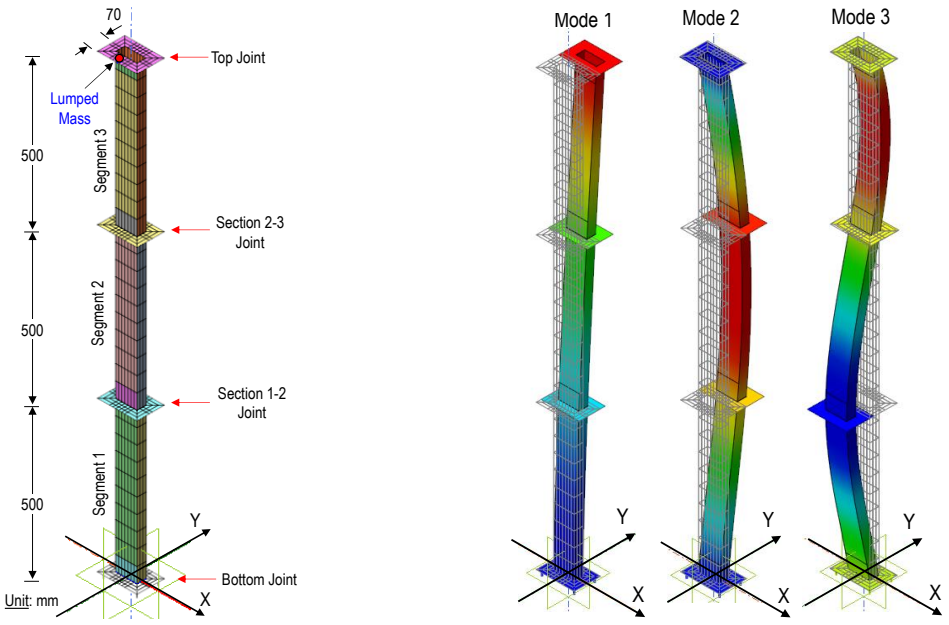

(a) 3D FE model (b) 3D bending mode-shapes

Fig. 8 Numerical modal analysis of the test structure

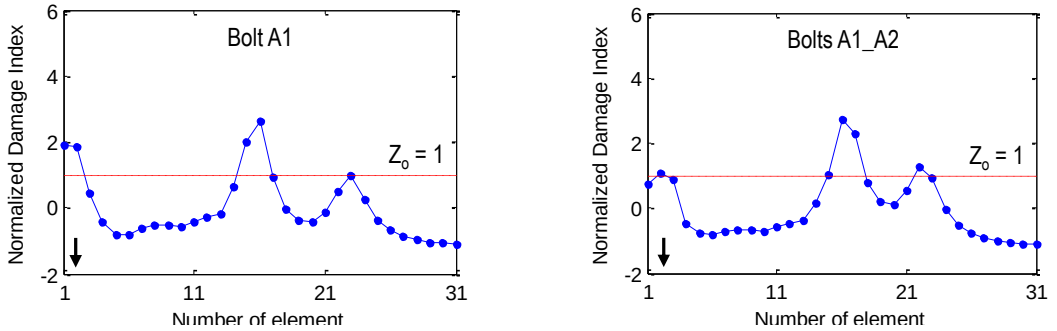

(a) Joint A (Bottom)

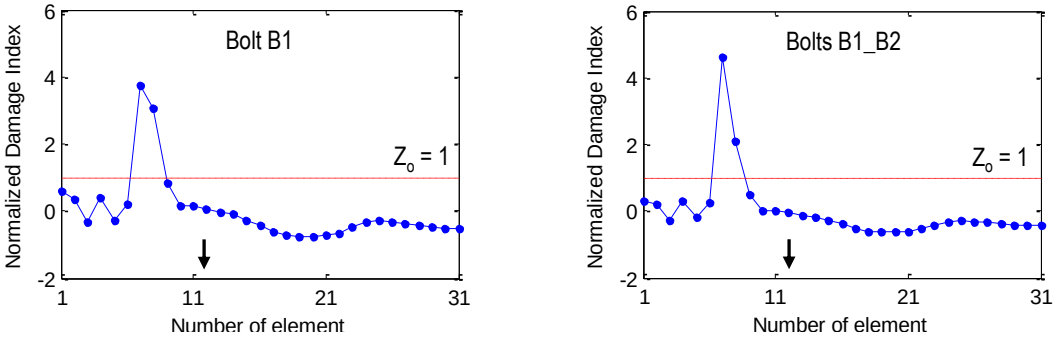

(b) Joint B (Section 1-2)

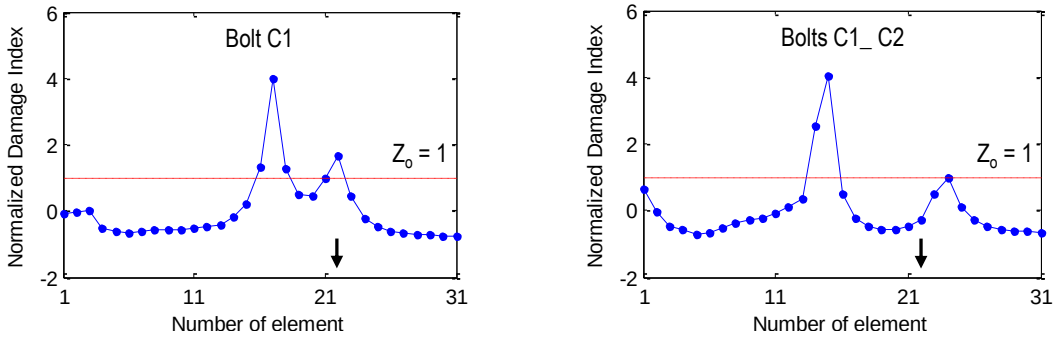

(c) Joint C (Section 2-3)

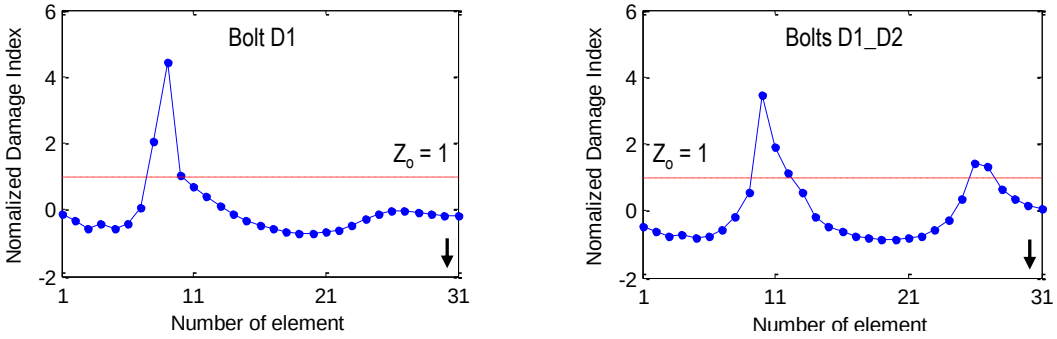

(d) Joint D (Top)

Fig. 9 Damage location estimation by frequency-based damage index
(↓: inflicted damage by bolt-loosening)

Table 3 Numerical natural frequencies of the FE model

	Natural frequency (Hz)		
	Mode 1	Mode 2	Mode 3
Simulation	2.2696	42.7251	104.1240
Experiment: Reference (A)	2.8243	40.1203	100.4870
Difference	19.6 %	6.5 %	3.6 %

The numerical natural frequencies of the three bending modes are listed in Table 3. The numerical frequencies were compared with the experimental ones for the intact case: Reference (A). It is observed that the frequencies of Mode 2 and Mode 3 are well-agreed between the numerical and the experimental models; the frequency differences are 6.5 % and 3.6 %, respectively. Meanwhile, the frequency difference between the two models for Mode 1 is relatively significant as 19.6 %. By adopting the Euler-Bernoulli beam theory, the tested model was considered as an equivalent cantilever beam with 31 elements. According to Eq. (9), the modal sensitivity, F_{ij}, was alternatively computed by using numerical mode-shape curvatures from FE model for three vibrational modes and 31 locations (i.e., 31 elements).

By implementing the relative changes in eigenvalues and the modal sensitivities obtained for the three bending modes and 31 elements, damage location estimation results were obtained from Eqs. (6)-(10), as shown in Fig. 9. Here, the threshold defined in Eq. (10) was set as equal 1 (Z_o=1) which was equivalent to the confidence level of 84%. Thereby, the damage was assigned to the location j^{th} if Z_j exceeds the confidence level.

As shown in Fig. 9(a), two damage cases simulated at Joint A (Bottom) were identified accurately. Accordingly, the predicted peaks were found precisely as compared to the inflicted location which was represented by equivalent-beam element #2. However, some false-predicted peaks were also observed in the middle of WT tower. For the damage cases at Joint B (Section 1-2), predicted zones were obtained at elements #7 and #8, which are a little far from the inflicted damage element (i.e., element #12) in both cases (see Fig. 9(b)). For damage cases at Joint C (Section 2-3), the location of damage case Bolt C1 was predicted with relatively good accuracy. Meanwhile, the location of damage case Bolt C2 was identified near the inflicted damage location (element #22). Similar to damage location estimation for simulated damage at joint A, the prediction errors were also observed at the mid-span, as performed in Fig. 9(c). For damage cases at joint D (Top), the location of both damage cases were predicted with relatively low accuracy. Thereby, for damage case Bolt D1, the frequency-based method was not able to predict the small damage at the free end. On the other hand, for damage case Bolt D1_D2, the most potential damage element was pointed at element #25 whereas the simulated damage location was inflicted at element #31, as shown in Fig. 9(d).

As observed in Fig. 9, some normalized damage indices at non-damage locations are greater than the threshold. The low accuracy prediction might be caused by the high stiffness of the segmental bolted joints in the WT tower that cause somewhat discontinuities in mode shapes and modal curvatures which were utilized for the damage localization.

4.4 Discussions on hybrid damage monitoring results

The experimental tests on the lab-scaled WT tower structure were intentionally conducted

Table 4 Summary of damage detection results of the proposed hybrid scheme

Damage location	Damage case	Stage 1	Stage 2		Stage 3	Hybrid SHM
		FRRAC	RMSD	CCD	Freq. Index	
Joint A (Bottom)	Bolt A1	O	Δ	Δ	□	Detectable
	Bolts A1_A3	O	Δ	Δ	□	Detectable
Joint B (Section 1-2)	Bolt B1	O	Δ	Δ	□	Detectable
	Bolts B1_B3	O	Δ	Δ	□	Detectable
Joint C (Section 2-3)	Bolt C1	O	Δ	Δ	□	Detectable
	Bolts C1_C3	O	Δ	Δ	□	Detectable
Joint D (Top)	Bolt D1	O	-	-	×	Fail
	Bolts D1_D3	O	-	-	□	Detectable

O: Damage is successfully alarmed
Δ: Damage is successfully classified as damage at bolted-connection joint
- : No available data
□: Damage location is detected
×: Damage is failed to detect

under the limited conditions including (1) the accelerometer was restricted in not only the number of sensors but also the arrangement; (2) only a few lower bending modes could be extracted from the vibration responses; (3) only three PZT sensors could be used for impedance measurement because the PZT sensor at the top joint was broken during installation process; and (4) damage could not be inflicted in the tower's segment by the sawed cutting.

With those given measurement data, the hybrid damage detection system using vibration and impedance responses was partially successful in detecting the damage in the lab-scaled WT model. It is observed from Fig. 5 that the vibration-based damage occurrence alarming was well-performed for the WT structure. Also, the impedance-based damage classification was successfully detected damage at the bolted-connection joint, as shown in Fig. 7. However, it is found that the location as well as the size of damage were predicted with relatively low accuracy. The unexpected results may be attributed to the inevitable errors caused by the data measurement as well as the modal parameter extraction processes. The results of the vibration- and impedance-based hybrid damage detection were summarized in Table 4. Although some predicted errors were observed in this experimental study, the proposed hybrid scheme is found to be potential for damage detection in the WT tower structure.

To enhance the damage prediction accuracy for this study and to be able to apply the proposed hybrid damage detection method for the real WT tower structure, at least four issues should be taken into consideration: (1) the number of sensors; (2) the sensor deployments; (3) the resolution of extracted modal parameters; and (4) the size and location of damage.

5. Conclusions

In this paper, a hybrid damage detection method for WT tower structures by measuring vibration and impedance responses was developed for WT tower structure. To achieve the

objective, the following approaches were implemented. Firstly, a hybrid damage detection scheme which combined vibration-based and impedance-based methods was proposed as a sequential process in three stages. Secondly, a series of vibration and impedance tests were conducted on a lab-scaled model of the WT structure in which a set of bolt-loosening cases was simulated for segmental joints. Finally, the feasibility of the proposed hybrid damage detection method was experimentally evaluated via its performance during the damage detection process in the tested model.

From the experimental evaluations, the following conclusions have been made. The FRRAC index computed from the vibration responses was good performance in alarming the occurrence of all damage cases inflicted in the WT tower structure. The damage simulated at critical member joints of the WT tower (i.e., bolt loosening at bolted-connection joint) was successfully detected by measuring the impedance responses. Thereby, the impedance-based damage monitoring technique was well-performed with damage classification jobs in the hybrid damage detection system. However, the damage location estimation had several errors under limited measurement data. The location of damage was predicted with relatively low accuracy. The combination of vibration and impedance-based methods provided a promising method for WT structures' health monitoring.

Despite the feasibility of hybrid damage monitoring scheme, some remaining works should be addressed in the future studies. For the real wind turbine structures, effects of uncertain conditions such as temperature, wind speed, and etc. on vibration and impedance responses can be significant which may result to false-alarms in the damage detection process. Therefore, the proposed hybrid damage monitoring system should be evaluated under many different wind excitations and temperature variation to calibrate its applicability in field monitoring.

Acknowledgments

This work was supported by the Pukyong National University Research Abroad Fund in 2012 (PS-2012-027).

References

Bang, H.J., Kim, H.I. and Lee, K.S. (2012), "Measurement of strain and bending deflection of a wind turbine tower using arrayed FBG sensors", *Int. J. Precision Eng. Manufact.*, **13**(12), 2121-2126.

Barazanchy, D., Martinez, M., Rocha, B. and Yanishevsky, M. (2014), "A hybrid structural health monitoring system for the detection and localization of damage in composite structures", *J. Sensors*, 1-10.

Bendat, J.S. and Piersol, A.G. (1993), *Engineering application of correlation and spectral ananlysis*, 2nd Ed., Wiley, New York.

Caithness Windfarm Information Forum (2016), "Summary of wind turbine accident data to 31 March 2016", *www.caithnesswindfarms.co.uk*.

Chiang, C.H., Hsu, K.T., Cheng, C.C., Pan, C.C., Huang, C.L. and Cheng, T.M. (2016), "Dynamic survey of wind turbine vibrations", *Proceeding of SPIE 9804*, Las Vegas, USA.

Chou, J.S. and Tu, W.T. (2010), "Failure analysis and risk management of a collapsed large wind turbine tower", *Eng. Fail. Anal.*, **18**(1), 295-313.

Corey Pitchford, Benjamin L. Grisso and Daniel J. Inman (2007), "Impedance-based structural health monitoring of wind turbine blades", *Proceeding of SPIE 6532, Health Monitoring of Structural and*

Biological Systems.
Dutton, A.G. (2004), "Thermoelastic stress measurement and acoustic emission monitoring in wind turbine blade testing", *European Wind Energy Conference*, London, UK.
Ebert, R. (2016), "Laser vibrometry for wind turbines inspection", *Proceeding of SPIE 9804,* Las Vegas, USA.
Han, X., He, Q., Sebastijanovic, N., Ma, T. and Yang, H.T.Y. (2007), "Developing hybrid structural health monitoring via integrated global sensing and local infrared imaging", *Proceeding of SPIE 6529,* San Diego, USA.
Huynh, T.C. and Kim, J.T. (2014), "Impedance-based cable force monitoring in tendon-anchorage using portable PZT-interface technique", *Math. Prob. Eng.*, 1-11.
Huynh, T.C. and Kim, J.T. (2016), "Compensation of temperature effect on impedance responses of PZT interface for prestress-loss monitoring in PSC girders", *Smart Struct. Syst.*, **17**(6), 881-901.
Ishihara, T., Yamaguchi, A., Takahara, K., Mekaru, T. and Matsuura, S. (2005), "An analysis of damaged wind turbines by Typhoon Maemi in 2003", *Proceeding of 6th Asia-Pacific Conference on Wind Engineering (APCWE-VI)*, 1413-1428.
Joosse, P.A., Blanch, M.J., Dutton, A.G., Kouroussis, D.A., Philippidis, T.P. and Vionis, P.S. (2002), "Acoustic emission monitoring of small wind turbine blades", *J. Solar Energy Eng.*, **124**(4), 446-454.
Kim, J.T., Na, W.B., Park, J.H. and Hong, D.S. (2006), "Hybrid health monitoring of structural joints using modal parameters and EMI signatures", *Proceeding of SPIE,* San Diego, USA.
Kim, J.T., Park, J.H., Hong, D.S. and Park, W.S. (2010), "Hybrid health monitoring of prestressed concrete girder bridges by sequential vibration-impedance approaches", *Eng. Struct.*, **32**(1), 115-128.
Kim, J.T., Park, J.H., Hong, D.S. and Ho, D.D. (2011), "Hybrid acceleration-impedance sensor nodes on Imote2-platform for damage monitoring in steel girder connections", *Smart Struct. Syst.*, **7**(5), 393-416.
Kim, J.T., Ryu, Y.S., Cho H.M. and Stubbs, N. (2003), "Damage identification in beam-type structures: frequency-based method vs mode-shape-based method", *Eng. Struct.*, **25**(1), 57-67.
Lading, L., McGugan, M., Sendrup, P., Rheinlander, J. and Rusborg, J. (2002), "Fundamentals for remote structural health monitoring of wind turbine blades-a preproject", *Annex E - Full-Scale Test of Wind Turbine Blade, Using Sensors and NDT*.
Law, S.S., Li, X.Y., Zhu, X.Q. and Chan, S.L. (2005), "Structural damage detection from wavelet packet sensitivity", *Eng. Struct.*, **27**(9), 1339-1348.
Lee, K.S., and Bang H.J. (2012), "A study on the prediction of lateral buckling load for wind turbine tower structures", *J. Precision Eng. Manufact.*, **13**(10), 1829-1836.
Liang, C., Sun, F.P. and Rogers, C.A. (1994), "Coupled electro-mechanical analysis of adaptive material - Determination of the actuator power consumption and system energy transfer", *J. Intel. Mat. Syst. Str.*, **5**, 12-20.
Liang, C., Sun, F.P. and Rogers, C.A. (1996), "Electro-mechanical impedance modeling of active material systems", *Smart Mater. Struct*, **5**(2), 171-186.
Matsuzaki, R. and Todoroki, A. (2006), "Wireless detection of internal delamination cracks in CFRP laminates using oscillating frequency changes", *Compos. Sci. Technol.*, **66**(3-4), 407-416.
Mostböck, A. and Petryna, Y. (2014), "Structural vibration monitoring of wind turbines", *Proceedings of the 9th International Conference on Structural Dynamics, EURODYN*, Portugal.
Nguyen, T.C., Huynh, T.C. and Kim, J.T. (2015), "Numerical evaluation for vibration-based damage detection in wind turbine tower structure", *Wind Struct.*, **21**(6), 657-675.
Overschee, V.P. and De Moor, B. (1996), *Subspace identification for linear system*, Kluwer Academic Publisher.
Park, G., Kabeya, K., Cudney, H. and Inman, D. (1999), "Impedance-based structural health monitoring for temperature varying applications", *Int. J. Series A Solid Mech. Mater. Eng.*, **42**(2), 249-258.
Park, J.H., Huynh, T.C., Choi, S.H. and Kim, J.T. (2015), "Vision-based technique for bolt-loosening detection in wind turbine tower", *Wind Struct.*, **21**(6), 709-726.
Pitchford, C., Grisso, B.L. and Inman, D.J. (2007), "Impedance-based structural health monitoring of wind turbine blades", *Proceedings of SPIE 6532,* San Diego, USA.

Qing, X., Kumar, A., Zhang, C., Gonzalez, I.F., Guo, G. and Chang, F.K. (2005), "A hybrid piezoelectric/fiber optic diagnostic system for structural health monitoring", *Smart Mater. Struct.*, **14**(3), 98-103.

Studer, M., and Peters, K. (2004), "Multiscale sensing for damage identification", *Smart Mater. Struct.*, **13**(2), 283-294.

Sun, F.P., Chaudhry Z., Liang, C. and Rogers C.A. (1995), "Truss structure integrity identification using PZT sensor-actuator", *J. Intel. Mat. Syst. Str.*, **6**(1), 134-139.

Tseng, K.K. and Wang, L. (2005), "Impedance-based method for nondestructive damage identification", *J. Eng. Mech.*, **131**(1), 58-64.

Zagrai, A.N. and Giurgiutiu, V. (2001), "Electro-mechanical impedance method for crack detection in thin plates", *J. Intel. Mat. Syst. Str.*, **12**(10), 709-718.

CC